Differential cross section for Na fine-structure transfer induced by Na and K collisions

P. W. Arcuni,* M. L. Troyer, and Alan Gallagher†
Joint Institute for Laboratory Astrophysics, National Institute of Standards and Technology and University of Colorado, Boulder, Colorado 80309-0440
(Received 11 September 1989)

The electronic energy-transfer process $Na^*(3P_{3/2})+M \rightarrow Na^*(3P_{1/2})+M$, where M is an Na or K atom, has been measured differentially with respect to scattering angle. This has been done with crossed beams and by establishing the final $(3P_{1/2})$ state velocity distribution from the Doppler spectrum of $3P_{1/2} \rightarrow 4D_{3/2}$ absorption. The differential cross section for Na perturbers is highly forward peaked (within a few degrees) with a small but extended high-angle tail. Forward angles are also dominant for K perturbers, but these cover a larger angular range with a very substantial large-angle contribution.

I. INTRODUCTION

Since the first "sensitized-fluorescence" measurements of $Hg^*+Tl \rightarrow Hg+Tl^*$ by Cario and Franck in 1923,[1] a great number of rate coefficients have been measured for such processes, which are now classified as "electronic energy transfer." These rate coefficients (k) span many orders of magnitude, depending on the specific species and states involved. This range of values can be understood in terms of the Landau-Zener-Stuckelberg equation for an electronic transition at an avoided level crossing, but real understanding of why a particular case has a particular value or magnitude is almost never achieved. This is due to the very strong dependence of k on the interatomic potentials and states of the diatomic collision complex, combined with an almost universal lack of knowledge regarding these critical characteristics. Thus, with the exception of certain alkali-metal–noble-gas transitions, the ensuing 60 years have provided neither definitive tests of theoretical understanding and approximations nor predictive capabilities.

Computers and calculational methods as well as molecular bound-state spectroscopy have advanced rapidly, so that meaningful molecular potentials and wave functions for many excited diatomic states can now be achieved. Indeed this has already happened for many alkali-metal–noble-gas[2–6] and alkali-metal–alkali-metal[7–11] pairs. Thus the basis now exists for a detailed understanding of atom-atom energy-transfer collisions to advance rapidly.

Experiments have been designed to obtain both more systematic and more detailed information than just the one number (k). The earliest systematic approach was by Krause and his collaborators, who in the 1950s and 1960s measured k for the alkali-metal fine-structure-changing transitions, for essentially the entire 4×5 array of alkali metals against noble-gas perturbers.[12] This was followed by measurements of very strong temperature dependencies of some of these k, a few years later in this laboratory.[13] Both observations were largely explained by Nikitin's models,[14] which also developed the molecular-recoupling description that is currently used in most theories of electronic energy transfer. Cross-section velocity dependencies have now been measured directly (rather than through T dependence) in cell[15] and in atomic beam experiments[16] for these same Na fine-structure transitions induced by noble-gas collisions as well as for collisions between pairs of excited Na atoms.[17]

Electronic energy transfer occurs unequally between different initial and final Zeeman states,[18] and this has also been exploited as a more detailed diagnostic. Schneider[19] made such measurements for the Na fine-structure changes due to noble-gas collisions, and Gough[20] demonstrated with $Hg^*+Cd \rightarrow Hg+Cd^*$ that it also holds for energy transfer to different atoms. Cross-section dependencies on the angle between the collision axis and the initial excited-state alignment have also been considered[16] and recently measured.[21,22]

Differential cross sections $Q(\theta)$ for elastic scattering of velocity-selected atomic beams can yield such highly detailed information that it can be almost uniquely inverted into the interaction potential. In the case of inelastic collisions, generally involving several adiabatic potentials connecting to each of the initial and final atomic states, there is no such "uniqueness." Nevertheless, there is still a great deal of information in a differential inelastic cross section, particularly if the transfer occurs predominantly through one pair of adiabatic states. Thus one would like to obtain such data as an exacting test of theories.

Differential cross sections for energy transfer in alkali-metal–alkali-metal collisions are particularly interesting. There are many molecular states involved, so that interesting theoretical issues such as axis rotation and nonadiabatic coupling arise. At the same time a great deal of information is available regarding the diatomic pair states and interaction energies.[7–11] Indeed, a very good approximation to the long-range A^*+B interactions and states, for all similar and dissimilar alkali-metal pairs, is obtained by diagonalizing a dipole-dipole plus fine-structure interaction matrix in which every parameter is known.[23] Higher-order corrections to this dipole-dipole interaction can also be evaluated from atomic pa-

rameters,[24] and in addition, many states of the close-range molecules are now well known from bound-state spectroscopy and *ab initio* calculations.[7–11] Energy defects span the space of 0.3–6000 cm^{-1} when transfer within and between alkali-metal atom pairs in the first excited state (nP_J) are considered. Thus this is an excellent system for a detailed investigation of many aspects of electronic energy-transfer collisions.

It is not an easy task to measure differential cross sections $Q(\theta)$ for short-lived excited states, but Phillips *et al.*[25] have developed a technique, which others have also used,[26,27] that can accomplish this. In particular, they studied the Na–noble-gas, fine-structure-changing problem utilizing a two-step velocity-selective excitation method similar to the method used by Liao, Bjorkholm, and Berman[28] to study velocity-changing kernels. Phillips *et al.* excited atoms of the Na beam to the $3P_{1/2}$ state, and when collisions with atoms of a noble-gas beam induced transfer to the $3P_{3/2}$ state, this was further excited optically to the $4D_{5/2}$ state and uv cascade fluorescence was detected (as in Fig. 1). The energy-transfer collision deflects the Na atom so that the $3P_{3/2}$ state velocity distribution is different than that of the original Na beam. This final-state velocity distribution is then seen as a Doppler-shift distribution when the probe laser ν_2 is tuned through the $3P_{3/2}$-$4D_{5/2}$ transition. For the orientation between the probe-laser beam and collision axis used in their experiment, the observed Doppler shift is proportional to $\cos\theta$, where θ is the center-of-mass scattering angle. Thus, in principle, this measures $Q(\theta)$. However, it is insensitive to $Q(\theta)$ near $\theta=0$ and 180°, where the Doppler shift is small and obscured by instrumental and hyperfine broadening. Phillips *et al.* avoided the associated data-inversion difficulties by calculating $Q(\theta)$ from a set of theoretical potentials and nonadiabatic coupling, then broadening this to account for experimental resolution and summing several overlapping hyperfine contributions. Satisfying agreement was found, although it is not clear what aspects of the theory were tested or how accurate the theory was in view of the several losses in resolution.

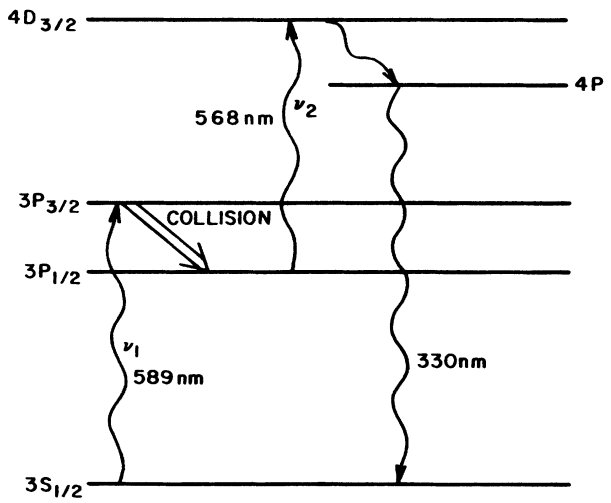

FIG. 1. Na energy levels and transitions involved in the present experiment.

Duren, Hasselbrink, and Hillrichs[26] and Mestdagh *et al.*[27] studied potassium fine-structure transfer due to noble-gas collisions, using the method of Phillips *et al.* Their experiments were also insensitive to θ near forward and backward angles, but sensitive to interesting $Q(\theta)$ oscillations at 40°–150°. Here also, theoretical $Q(\theta)$ were broadened to compare with experimental spectra.

The experiment reported here extends the method of Phillips *et al.* to a full determination of the differential cross section at small scattering angles, essentially free of experimental broadening and hyperfine overlap. We have measured the same Na $3P_{3/2}\rightarrow 3P_{1/2}$ fine-structure transfer, but due to collisions with other alkali-metal atoms rather than noble gases. That is, we do a state-to-state differential measurement of the following two reactions:

$$Na^*(3P_{3/2})+Na(3S_{1/2})\rightarrow Na^*(3P_{1/2})+Na(3S_{1/2}) , \quad (1)$$

$$Na^*(3P_{3/2})+K(4S_{1/2})\rightarrow Na^*(3P_{1/2})+K(4S_{1/2}) . \quad (2)$$

The initial $3P_{3/2}$ state is a mixture of hyperfine components $F=3,2,1$ that is dominated by $F=3$. The final state contains two hyperfine states $F=2,1$, which are partially resolved. Due to the symmetry of the Na beams, we do not distinguish between the reaction shown in Eq. (1) and the reaction $Na^*+Na\rightarrow Na+Na^*$. In the following we introduce the measurement method, then details of our experimental conditions, describe the data analysis, and finally, discuss the resulting $Q(\theta)$.

II. MEASUREMENT METHOD

Our experimental arrangement is shown diagrammatically in Fig. 2, the optical transitions utilized are in Fig. 1, and a center-of-mass representation of the atomic-motion and probe-laser-beam directions is shown in Fig. 3. Alkali-metal beams A and B intersect at 90° and laser beam 1, of frequency ν_1, excites beam A from $3S_{1/2}$ ($F=2$) to $3P_{3/2}$ (mostly $F=3$). (Beams A and B have opposite ν_1 Doppler shifts, so only one is excited by the laser frequency ν_1.) Na atoms that have been collisionally transferred from the $3P_{3/2}$ to $3P_{1/2}$ state are further excited to the $4D_{3/2}$ state by a probe laser of frequency ν_2. In our experiment the probe-laser beam propagates perpendicular to the scattering plane. The reason for using this configuration, which has not previously been utilized, will be discussed in the next paragraph. The cascade fluorescence from a fraction of the atoms that have been excited to the $4D_{3/2}$ state is detected. The collisional $3P_{3/2}$ to $3P_{1/2}$ energy transfer deflects the Na atoms, so the $3P_{1/2}$-$4D_{3/2}$ excitation is observed with a Doppler shift of $\Delta\nu_D=\tilde{\mathbf{v}}'_A\cdot\hat{\mathbf{z}}'/\lambda$, where $\hat{\mathbf{z}}'$ is the ν_2 laser beam direction and $\tilde{\mathbf{v}}_A\cdot\hat{\mathbf{z}}'=0$. In Fig. 3 this is shown in center-of-mass (c.m.) coordinates for atoms of beam A only, as is appropriate for the dissimilar-atom case, Eq. (2). In the identical-atom case, Eq. (1), both beams are identically and symmetrically deflected in the z' direction, so considering beam A alone is equally satisfactory

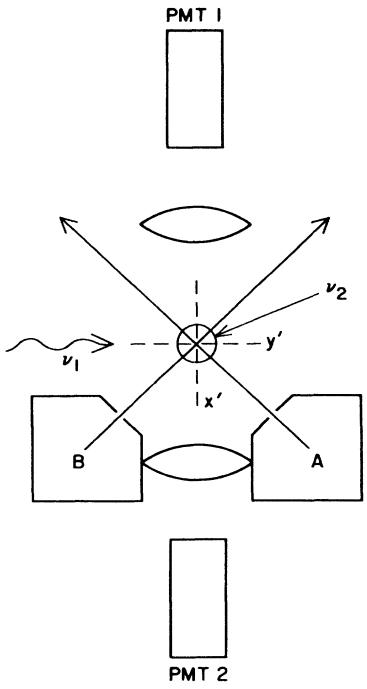

FIG. 2. Diagrammatic representation of the horizontal scattering plane of the experiment. The probe (ν_2) laser beam propagates downward, perpendicular to this plane. Center-of-mass coordinates x' and y' are shown for the Na^*-Na case.

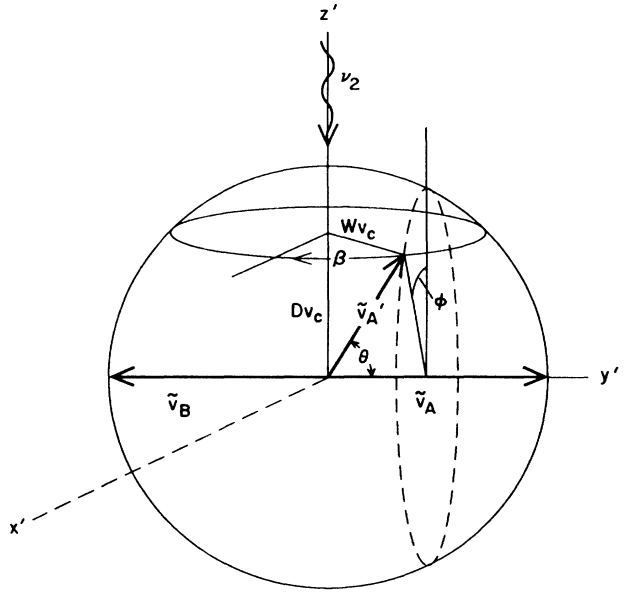

FIG. 3. Center-of-mass velocities of atoms from beam A and beam B before collision ($\bar{v}_A, \bar{v}_B$), and of beam A after the collision ($\bar{v}'_A$). The center-of-mass scattering angles are θ and ϕ, and $v_C = |\bar{v}_A|$.

In Fig. 3, and in Fig. 2 for the Na^*+Na case, the scattering is shown in a primed coordinate system, rotated about $\hat{z}$ relative to the laboratory coordinates to place $\bar{v}_{c.m.}$ along x' and the initial $\bar{v}_{relative}$ along y'. It is apparent from Fig. 3 that a probe laser propagating along y' detects a collisional Doppler shift of $(\bar{v}_A - \bar{v}'_A)\cdot\hat{y}'/\lambda = |\bar{v}_A|\lambda^{-1}(1-\cos\theta)$. This has the distinct advantage, for initially unoriented atoms that scatter equally into all ϕ, that all ϕ are detected simultaneously.[25] On the other hand, it has some serious disadvantages. The Doppler shifts are very small for small-angle scattering, and these collisional Doppler shifts are superimposed on the initial beam excited-state velocity spread. The natural linewidth of the $3P_{3/2}$ state of Na limits the excited atom velocity spread to 1.5% in the absence of power broadening or multiple hfs components. For the experiments reported here, where most scattering is less than 3°, this velocity spread produces a Doppler width of ~20 times the entire collisional Doppler spread in the y' direction. Thus, whereas previous experiments have been done in this configuration, it would yield no useful information here. In essence, previous experiments have not been sensitive to the form of $Q(\theta)$ for θ near 0° and 180°, but were very sensitive near $\theta \sim 90°$ and to forward-backward asymmetry. In contrast, the present probe-beam geometry ($\hat{k}_2 = \hat{z}$) is sensitive to θ near 0°, is insensitive to θ near 90°, and does not detect forward-backward asymmetry.

An important advantage of the present probe-beam arrangement is that the initial ($3P_{3/2}$ state) beam velocity spread in the probe direction is fixed by beam collimation rather than the linewidth and hfs of the ν_1 transition. Thus, in the present case the residual beam Doppler width, on which the collisional broadening is superimposed, is independent of ν_1 laser power and can be made as narrow as needed. In contrast, in the $\hat{k}_2 = y'$ case, several partially resolved hyperfine velocity groups are excited, each with a different power-dependent velocity width and size.

From Fig. 3 it can be seen that when $\hat{k}_2 = \hat{z}'$ a range of θ values contribute to the signal at one $\Delta\nu_2$. Extracting $Q(\theta)$ from $P(\nu_2)$, the signal versus ν_2, thus requires a deconvolution using a weighted integral of $d[P(\nu_2)]d\nu_2$ that is similar to the Abel inversion but with a different weighting. This case has been analyzed by Serri, Kinsey, and Pritchard[29] so we only summarize their result.

They have shown that when the observed signal is expressed in terms of a new frequency variable $D = \Delta\nu_2\lambda/|\bar{v}_A|$, that varies from +1 to −1, then

$$P(D) = K\int_0^W \Sigma(\theta)(W^2-\cos^2\theta)^{-1/2}d(\cos\theta)\,, \qquad (3)$$

where $W = (1-D^2)^{1/2}$, $\Sigma(\theta) = \sigma(\theta)+\sigma(\pi-\theta)$ is the "folded" cross section, and K is a proportionality constant. Equation (3) can be inverted[29,30] to obtain $\Sigma(\theta)$ from $P(D)$ using either Eq. (7) or Eq. (19) of Serri, Kinsey, and Pritchard. We repeat their Eq. (7) here to show that this involves an integration and then differentiation of the data

$$\Sigma(\theta) = (K\pi)^{-1}\frac{d}{d(\cos\theta)} \times \left[\int_{W=0}^{\cos\theta} W(\cos^2\theta - W^2)^{-1/2}P(D)dW\right]. \qquad (4)$$

TABLE I. Atomic beam parameters.

Parameter	Na+Na (Expt.)	Na+K (Expt.)
$\bar{v}_A$[a]	1000 m/s	1120 m/s
$\bar{v}_B$	1000 m/s	630 m/s
$\delta v_A/v_A$[b]	0.15	0.15
$\delta\nu_2$[c]	55 MHz	55 MHz

[a]This is the center-of-mass velocity.
[b]δv_A is the rms velocity spread.
[c]$\delta\nu_2$ is the rms width.

In the Na*+Na case, symmetry requires $\sigma(\theta)=\sigma(\pi-\theta)$, and in this as well as the Na*+K case $\Sigma(\theta)\cong\sigma(\theta)$ because forward scattering dominates.

Serri, Kinsey, and Pritchard[29] derived an approximate formula for the expected angular resolution using $\hat{\mathbf{k}}_2=\hat{\mathbf{z}}'$. We repeat it here, with a minor correction,

$$(\delta\theta)^2=\left[\frac{2\delta\nu_2}{[(v_A+v_B)/\lambda_2]\cos\theta}\right]^2+\frac{2[(\delta v_A)^2+(\delta v_B)^2]}{(v_A+v_B)^2}\sin^2\theta\ . \quad (5)$$

In this equation, v_A and v_B are the magnitudes and δv_A and δv_B are the root-mean-square velocity spreads of the y'-directed velocity of beams A and B. $\delta\nu_2$ is the root-mean-square width of the probe transition due to natural and power-broadening linewidth plus the residual z-direction Doppler width. Our relevant experimental parameters, for both reactions [Eqs. (1) and (2)], are listed in Table I and will be discussed in the next section. Substitution of these values into Eq. (5) results in the $\delta\theta$ resolution shown in Fig. 4. A higher resolution than this $\sim 2°$ is needed for Na*+Na collisions, since small-angle scattering dominates. As described below, we have achieved higher resolution by measuring and deconvolving the experimental width $\delta\nu_2$ from the signals. The resolution is then limited by the velocity-spread part in Eq. (5). As seen in Fig. 4, this is much smaller for $\theta<10°$.

III. EXPERIMENTAL APPARATUS

A schematic view of our experimental apparatus is shown in Fig. 2, and the optical and collision-induced transitions are shown in Fig. 1. The two ovens A and B produced supersonic alkali-metal beams, typically with a fractional velocity spread of $\sim 30\%$. The Na ovens were typically operated at ~ 800 K, and the potassium oven at ~ 700 K. A 1.3-mm-diameter, oven-temperature skimmer 1.7 cm from each ~ 0.2-mm oven orifice initially collimated the beams. A ~ 200 °C aperture further collimated beam A to a horizontal, ribbon-shaped cross section with 2.0-mm-long dimension and 0.6-mm-short (z) dimension in the interaction region 5.5 cm from the oven. This fixed the z angular divergence at $\sim 0.7°$. Beam B had a ~ 5.0-mm-diameter circular cross section in the collision region to ensure intersection with beam A. The average collision energy for these 90°-intersecting supersonic beams was ~ 0.24 eV.

The ν_1 laser beam, from a dye laser, was in the horizontal plane at 45° to each atom beam, and had a linewidth of ~ 1 MHz and typical power density of 80 mW/cm^2. It could be continuously scanned across each of the Na D lines. The fluorescence resulting from the D-line excitation was focused by a lens onto a photomultiplier, PMT1 in Fig. 2. An example of the resulting fluorescence spectra (with only 2 μW/cm^2 laser power) is shown in Fig. 5. In this example both ovens contained Na and the laser was scanned across the D_2 line $3S_{1/2}\rightarrow 3P_{3/2}$. The four lines are two pairs of 1772-MHz-separated Na($3S_{1/2}$) hyperfine transitions. The pair from beam A is Doppler shifted to a lower ν_1 resonance and the pair from beam B to a higher resonance. The intensity difference between the two beams is due to the larger physical size of beam B. Absorption measurements showed that the two alkali-metal beams had the same density, $\sim 8\times 10^{10}$/cm^3. From Fig. 5 we determine the beam velocity and the full width at half-maximum (FWHM) velocity spread. These beam parameters are listed in Table I.

We have much less knowledge about the conditions of the K beam, but since we did not laser probe it, these are

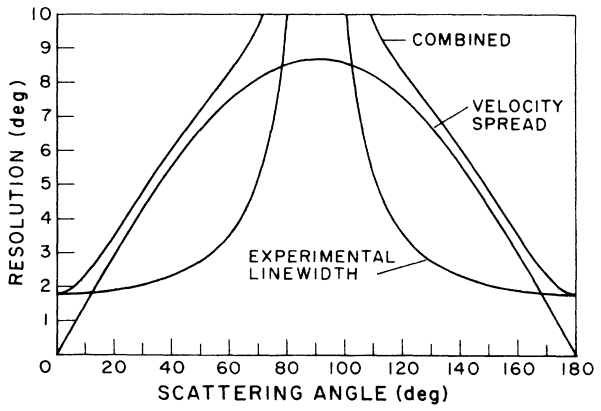

FIG. 4. Angular resolution of the experiment due to natural linewidth and power broadening and beam velocity spread, assuming no deconvolution procedures.

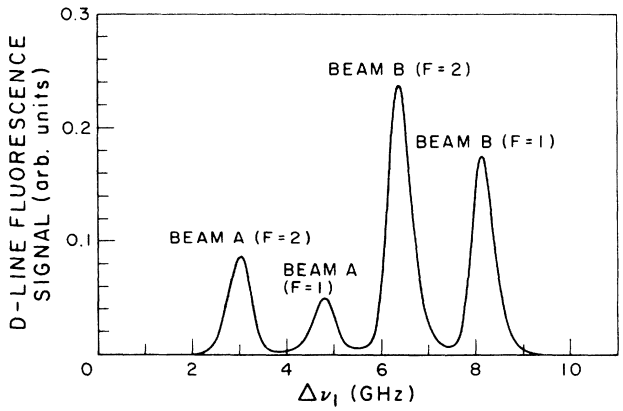

FIG. 5. Na $3P_{3/2}$ 589-nm fluorescence vs ν_1 for beams A and B.

not critical for the analysis. Nevertheless, from the approximate pressure and temperature inside the oven, and assuming that Na and K behave similarly in their adiabatic expansion from the oven nozzle, we have made estimates that are also displayed in Table I.

The second, downward-directed probe-laser beam (ν_2) was also from a cw dye laser with a linewidth of ~ 1 MHz. We typically utilized about 20 mW/cm^2. This laser excited the $3P_{1/2} \rightarrow 4D_{3/2}$ transition, and $\sim 15\%$ of the excited atoms cascade through the $4P \rightarrow 3S$, 330-nm transition. This uv light was focused by a quartz lens onto a bialkali-metal photomultiplier, and the detected photons were digitally counted.

The ovens and beams were contained in a diffusion-pumped vacuum chamber, maintained at $\sim 3 \times 10^{-7}$ Torr. Each oven was surrounded by a water-cooled copper box, and most of the escaping alkali metal condensed on the interior surfaces of these boxes. Additional large copper plates, indirectly cooled by liquid nitrogen, enhanced alkali-metal condensation. Nonetheless, there was evidence of a significant amount of Na (or Na and K) background vapor in the collision region. This background Na could cause fine-structure changing collisions that were independent of the presence of beam 2, and typically 20% of the crossed-beam signal. We therefore used a shutter to turn beam 2 on and off, and the reported crossed-beam signal is the difference between the signal with shutter open and closed. (This shutter was in the main chamber, so it did not effect the total beam flux into the chamber and thus the background.)

IV. DATA

To measure the instrumental line shape, we measured a "no collision signal." Here, the ν_1 laser was tuned to the $3S_{1/2}$ $(F=2) \rightarrow 3P_{1/2}$ transition of beam A, which excited both $F=1$ and 2 of $3P_{1/2}$ due to the beam velocity spread. The ν_2 laser then excited the $3P_{1/2} \rightarrow 3D_{3/2}$ transition. The 330-nm signal resulting from this two-photon resonant process is shown in Fig. 6. The two peaks are from the hyperfine levels of the $3P_{1/2}$ state; they each have a FWHM of ~ 35 MHz and a rms width of 55 MHz. This width is due to the natural width of the probe transition (~ 13 MHz), beam angular divergence (~ 27 MHz), and a minor amount of probe-transition power broadening.

The 330-nm collision signals versus $\Delta\nu_2$ are also shown in Figs. 6 and 7, where they are labeled $S(\Delta\nu_2)$. The Na*+Na signal is the average of ten scans. The Na+K is averaged over three scans; the latter signal was weaker due to the smaller cross section and noise is apparent. The greater width of the transfer signals, compared to the two-photon signal, is due to the collisional scattering and will be used to obtain $Q(\theta)$. Note that the resonant Na*+Na fine-structure transition has less width than the nonresonant Na*+K process, as expected for longer-range Na*+Na process. When the hfs is allowed for, as shown in Fig. 7, the Na*+K signal cuts off at approximately ± 2.0 GHz and the Na*+Na signal at approximately ± 1.7 GHz, corresponding to 90° deflection. We calculate, using the Na- and K-beam parameters in Table

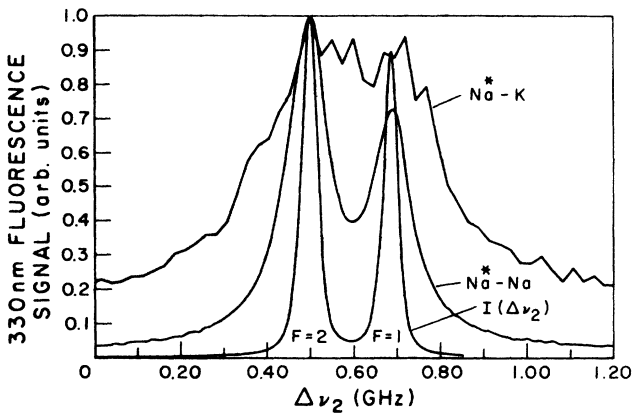

FIG. 6. 330-nm fluorescence vs ν_2. The narrow line labeled $I(\Delta\nu_2)$ is from optical excitation of the $3P_{1/2}$ state, the result of the Na*+Na collisional population of the $3P_{1/2}$ state is so labeled, and the wide, noisy line results from Na*+K collisions.

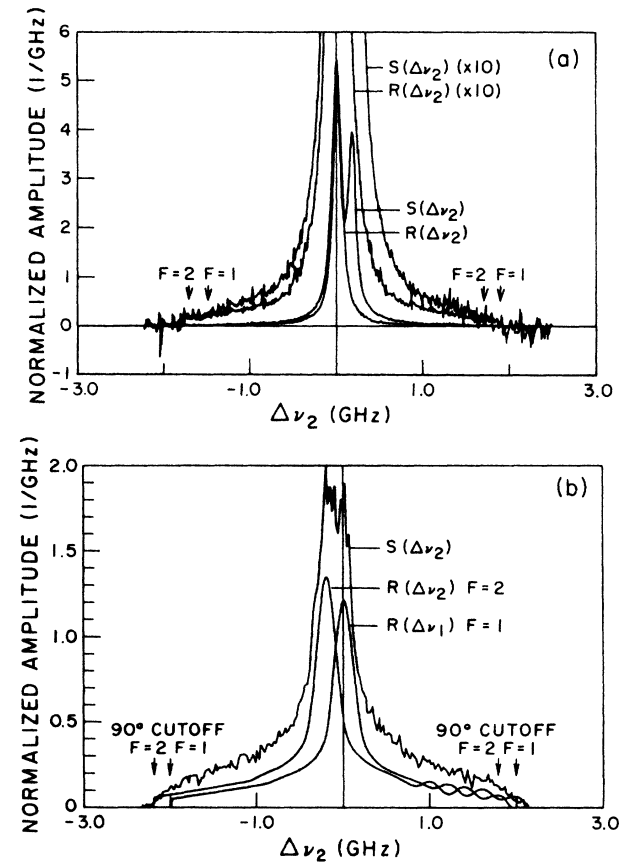

FIG. 7. (a) $S(\Delta\nu_2)$ is the signal due to Na*+Na collisions and contains both $3P_{1/2}$ hyperfine states $(F=2,1)$. $R(\Delta\nu_2)$ is the contribution from just one hyperfine state $(F=2)$. Both are also shown ($\times 10$). (b) $S(\Delta\nu_2)$ is the signal due to Na*+K collisions. $R(\Delta\nu_2)$ is shown for each hyperfine state contribution $(F=2,1)$. The oscillations in the positive $\Delta\nu_2$ wing of $R(\Delta\nu_2)$ for $F=2,1$ are from the Fourier separation technique. A smooth curve drawn through these oscillations is shown in the negative $\Delta\nu_2$ wing; this is the $R(\Delta\nu_2)$ used in further analysis. The arrows show the cutoff of the signal at (a) ± 1.7 GHz for Na*+Na and (b) ± 2.0 GHz for Na*+K due to 90° scattering along z'.

I, that this Na^*+K cutoff should occur at ± 1.9 GHz and the Na^*+Na at ± 1.7 GHz. We consider this good agreement, particularly in view of the relatively poor signal size at the cutoff frequencies and the uncertainty in K-beam parameters.

The contribution of dimers to our observed signals is expected to be negligible. At our experimental conditions, we estimate $\sim 5\%$ Na_2 in the Na beam and $\sim 1\%$ K_2 in the K beam.[31,32] In the Na^*+Na case of Eq. (1), the long-range C_3/R^3 resonant interaction causes a much larger cross section than in the nonresonant case of dissimilar alkali metals.[33] We expect the same behavior for the nonresonant Na^*+Na_2 case. In the dissimilar-atom case of Eq. (2), the cross section for collisions involving $Na+K_2$ should be of the same order of magnitude as for Na+K. When we take into account the ratio of the nonresonant to resonant cross sections ($\sim 15\%$), the fraction of the differential cross section which is found at $\theta > 45°$ ($\sim 3\%$ for Na^*+Na and $\sim 25\%$ for Na^*+K), and the small fraction of Na_2 and K_2 in the beams, we conclude that little of our signal comes from dimer contributions.

V. DATA REDUCTION

We now deconvolve the data $S(\Delta\nu_2)$ shown in Figs. 6 and 7 to obtain the differential cross sections. There are several steps to this. First, the hyperfine structure must be accounted for. Second, the experimental broadening observed in the two-photon process must be removed. Finally, the cross section must be extracted using the inversion Eq. (4). This procedure is now described.

A. Na^*+Na collision data

To separate the hyperfine contributions seen in the $3P_{1/2}$ excitations we note that the $3P_{1/2}$ $(F=2)$ and $(F=1)$ hyperfine states are separated by 189 MHz while the hyperfine splitting of the $4D_{3/2}$ state is <3 MHz and can be neglected. We assume that $\sigma(\theta)$ is the same for collisional energy transfer to each $3P_{1/2}$ hyperfine state, so that the signal $S(\nu_2)$ from each hyperfine component is $R(\nu_2)$ with a relative scaling factor A and a frequency shift B,

$$S(\nu_2)=R(\nu_2)+AR(\nu_2+B)\ , \tag{6}$$

where A is determined by data fitting and $B=189$ MHz. $R(\nu_2)$ is then obtained by Fourier transform methods

$$R(\nu_2)=F^{-1}\left[\frac{F(S(\nu_2))}{[1+A\exp(i2\pi\nu_2 B)]}\right]\ , \tag{7}$$

where F is the Fourier-transform operator and F^{-1} is the inverse operator. Symmetry arguments require $R(\Delta\nu_2)$ to be symmetric, and we symmetrize it by using only symmetric cosine functions in Eq. (7). In essence, this averages data with positive and negative detuning. The resulting $R(\nu_2)$ are shown in Fig. 7. Since these $3P_{1/2}$ state hyperfine levels are primarily populated from the $3P_{3/2}$ $(F=3)$ level, the ratio A need not be the statistical ratio of 0.6; we obtain 0.68 from the Na^*+Na data in Figs. 6 and 7. The same process is used to obtain a single peak $I(\Delta\nu_2)$ shown in Fig. 8 from the two hfs instrumental peaks shown in Fig. 6.

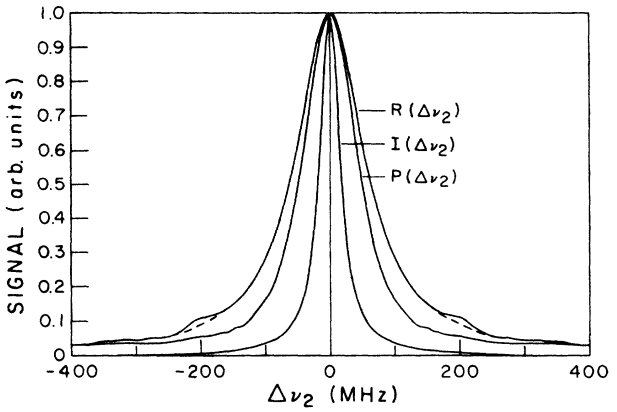

FIG. 8. $R(\Delta\nu_2)$ signal, corresponding to the experimental signal for a single hyperfine component of the $3P_{1/2}$ state. $I(\Delta\nu_2)$ is the instrumental signal for a single hyperfine peak, and $P(\Delta\nu_2)$ is the collisional portion of the Na^*-Na signal. The small bumps in $R(\Delta\nu_2)$ at ± 200 MHz are due to incomplete hyperfine separation.

In Fig. 8 we show the $R(\Delta\nu_2)$ signal from the Na^*+Na energy-transfer process. The small bumps in $R(\Delta\nu_2)$ at ± 200 MHz are due to incomplete hfs separation. The dashed line shows the assumed actual shape corresponding to complete separation. We now take the observed Na^*+Na fluorescence to be a convolution of the instrumental response $I(\Delta\nu_2)$ and the true scattering signal $P(\Delta\nu_2)$, where the latter is equivalent to $P(D)$ in Eqs. (3) and (4),

$$R(\Delta\nu_2)=\int_{-\infty}^{\infty} P(\nu')I(\Delta\nu_2-\nu')d\nu'\ . \tag{8}$$

From the Fourier-transform convolution theorem,

$$F(R(\Delta\nu_2))=F(P(\Delta\nu_2))F(I(\Delta\nu_2))\ . \tag{9}$$

$P(\Delta\nu_2)$ is then obtained by the deconvolution

$$P(\Delta\nu_2)=F^{-1}[YF(R(\Delta\nu_2))/F(I(\Delta\nu_2))]\ , \tag{10}$$

where

$$Y=[1+(x/x_0)^{2N}]^{-1/2} \tag{11}$$

is a Butterworth filter used to reduce high-frequency noise, N is the order of the filter, and x_0 is the cutoff in Fourier space. Frequencies greater than x_0 are thus attenuated, while frequencies below x_0 are changed little and signal changes with $\Delta=1/(2\pi x)$ spacing are averaged over. Typical parameters used were $N=4$ and $x_0=0.025$ MHz^{-1}, corresponding to a $\Delta=7$-MHz averaging width. $P(\Delta\nu_2)$, shown in Fig. 8, represents the velocity distribution of $3P_{1/2}$ state atoms, perpendicular to the scattering plane, that is produced by collisional energy transfer.

The final step is the inversion of $P(\Delta\nu_2)$ to $Q(\theta)$. To use the inversion equation, Eq. (4), we change the

frequency coordinates of $P(\Delta\nu_2)$ to $P(D)$ using $D=\Delta\nu_2/1.7$ GHz for Na*+Na. The $Q(\theta)$ result of the inversion process is shown in Fig. 9, where we also show what would have been obtained if we had not deconvolved the "instrumental response function" from the data.

The fairly regular fluctuations in the 5°–20° region in Fig. 9(b) are consequences of statistical noise that is accentuated by the Eq. (4) inversion, and made semiregular by the high-frequency filtering in Eq. (10). This filtering also removes any rapid $\sigma(\theta)$ fluctuations that might exist; these are already removed from the present data by velocity smearing.

In order to estimate the accuracy of this $\sigma(\theta)$ result, a small portion of the $P(\Delta\nu_2)$ data was bounded by two Lorentzian curves, as is shown in Fig. 10(a). These two curves, along with a Lorentzian fit to the data and the data itself, were analyzed by the above procedures, with the results shown in Fig. 10(b). The inversion procedure appears to be stable and essentially transforms fractional fluctuations in $P(\nu_2)$ into equivalent fractional fluctuations in $\Sigma(\theta)$. This fortunate behavior is a consequence of the relatively sharp kernel $[(\cos^2\theta-W^2)^{-1/2}]$ in Eq. (4).

B. Na*+K collision data

Due to the poor signal-to-noise ratio, a slightly different procedure was used to obtain the differential cross section for the Na*+K case. As before, the individual hyperfine components $R(\Delta\nu_2)$ are first extracted with Eq. (7). As the result was fairly noisy, a Butterworth filter averaging over $\Delta\cong 7$-MHz intervals was used to smooth the resulting $R(\Delta\nu_2)$ data. Since the width of this $R(\Delta\nu_2)$ is considerably broader than for Na*+Na, and $I(\nu_2)$ deconvolution increases noise, we did not deconvolve the two-photon peak, i.e., we take in place of Eq. (10),

$$P(\Delta\nu_2)\cong F^{-1}(YF(R(\Delta\nu_2)))\ . \tag{12}$$

This $P(\Delta\nu_2)$, shown at positive $\Delta\nu_2$ in Fig. 7(b), contains significant oscillations in the far wings; these are artifacts of the noisy signal and the filtering. A smooth curve, shown at negative $\Delta\nu_2$, was thus fit through the oscillations, with a sharp cutoff at the 90° scattering frequency of 2.0 GHz. This smoothed $P(\Delta\nu_2)$ was then inverted with Eq. (4) to obtain $\Sigma(\theta)$, which is shown in Fig. 9. Based on the data in Fig. 8 and the Fig. 9(a) comparison of $Q(\theta)$ for Na*+Na, obtained with and without instrumental broadening, we estimate that not deconvolv-

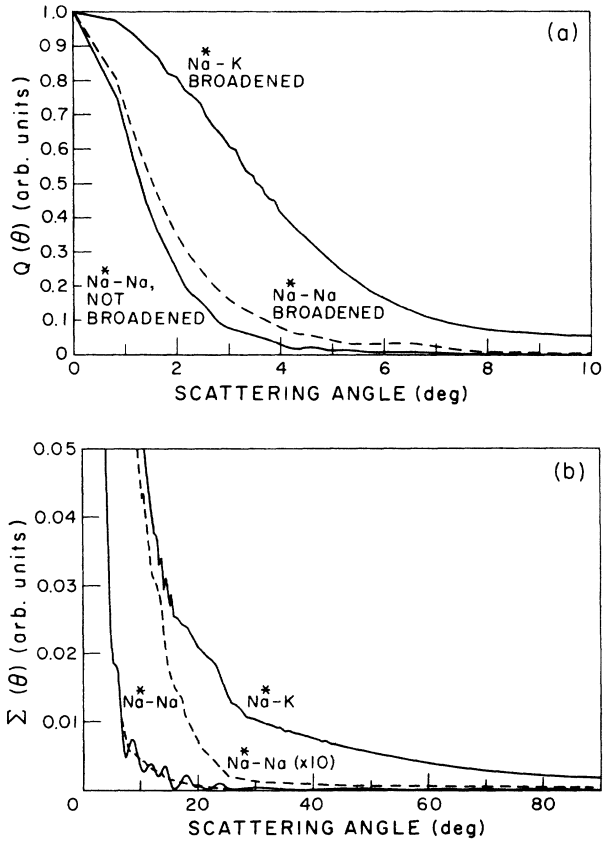

FIG. 9. Differential cross sections $Q(\theta)$ for Na*+Na and Na*+K collisions. The dashed line in (a) represents the Na*+Na result obtained when instrumental broadening is not removed. Parts (a) and (b) show different θ regions. The dashed lines in (b) are an average through small oscillations attributed to the inversion procedure.

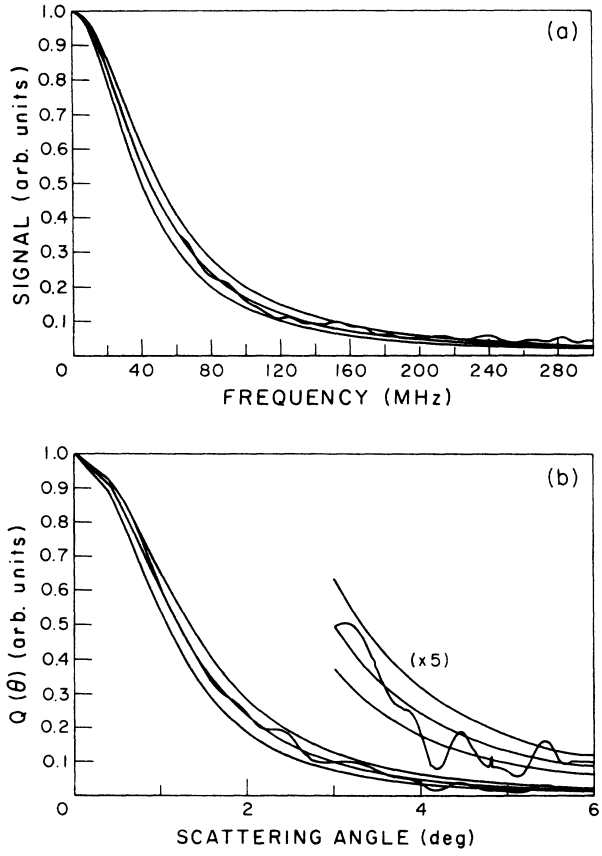

FIG. 10. (a) Typical $P(\Delta\nu_2)$ data for the Na*+Na case (wavy line) and three bracketing Lorentzians. (b) $Q(\theta)$ obtained by inverting the four $P(\Delta\nu_2)$ in part (a).

ing the experimental resolution has increased the width of $\Sigma(\theta)$ for Na^*+K by $\sim 7\%$. Note the significant large-angle scattering in the Na^*+K collision system.

VI. CONCLUSIONS

We have been able to show that $Q(\theta)$ can be obtained from our experimental data with good resolution at small angles. This has been achieved by deconvolving the experimental line shape, due to residual velocity spread along the probe-laser beam direction plus natural linewidth and power broadening, from the experimental data. As seen from Fig. 4, the angular resolution $\Delta\theta$ then improves to $\sim\theta/7$ for small angles, where this resolution limit is due to the velocity spread of the beams in their propagation directions. This improvement in resolution was crucial for the Na^*+Na case where the cross section was highly peaked below 2°.

The observed cross sections $\Sigma(\theta)$ for Na^*+Na and Na^*+K were both found to be highly peaked at small angles. For Na^*+Na, when weighted by solid angle $d\Omega$, $\sim 75\%$ of $\Sigma(\theta)\,d\Omega$ is between $\theta=0°$ and 5°, which corresponds to atoms scattered at impact parameters larger than ~ 25 Å by the C_3/R^3 resonant interaction of Na^*+Na. In contrast to this, though the Na^*+K case is still peaked near $\theta=0°$, $\sim 25\%$ of $\Sigma(\theta)$ is at $\theta<5°$. This corresponds to atoms scattered by the C_6/R^6 interaction at impact parameters greater than ~ 8 Å. In fact, $\sim 25\%$ of the total $\Sigma(\theta)$ is found at $\theta>45°$. In contrast, only $\sim 3\%$ of $\Sigma(\theta)$ is at $\theta>45°$ for the Na^*+Na case. In essence, a major fraction of the Na^*+K reaction is due to large-angle scattering, while only a very small fraction of the Na^*+Na reaction is due to large-angle scattering.

Although the alkali-metal-pair potentials are exceptionally well known and calculable, we are not aware of any collision-dynamics calculations of the differential cross sections reported here. We hope this paper will stimulate some interest in them. It is clear that as the theory advances and justifies the effort, angular and spin-dependent differential cross sections could be measured by small modifications of the present experiment. This would help separate the role of different interatomic states in the energy transfer. By changing the beam collision angle, the collision energy can also be varied by large factors. Thus developments based on the experimental method of Phillips *et al.* can be very exacting probes of collision theory as well as of interatomic potentials.

Spectroscopic probing of the short-lived final state of a collision has an overall detection efficiency of $\sim 10^{-4}$ in the present experiment. For our beam densities of $\sim 10^{11}$ cm^{-3}, a typical energy-transfer rate coefficient of 10^{-10} $cm^3\,s^{-1}$ and an excited-state lifetime of 10^{-8} s, one signal photoelectron is detected for $\sim 10^{11}$ Na excitations. The atom flux through the ν_1 laser beam is $\sim 10^{14}$/s and an average atom is excited a few times before being hyperfine pumped, so the photoelectron count rate is $\sim 10^3$/s. It would be quite feasible to decrease the optical-pumping loss and increase the fluorescence collection efficiency. These numbers are characteristic of many feasible experiments, and they show that differential, energy-transfer cross sections can be measured for many short-lived excited states by this method. The data reduction performed here also shows that unique differential cross sections with high angular resolution can be obtained directly from such data.

ACKNOWLEDGMENTS

This work was supported by National Science Foundation Grant No. PHY86-04504 through the University of Colorado.

*Present address: Department of Physics, Notre Dame University, Notre Dame, IN 46556.
†Quantum Physics Division, National Institute of Standards and Technology.

[1]G. Cario and J. Franck, Z. Phys. **17**, 202 (1923).
[2]W. E. Baylis, J. Chem. Phys. **51**, 2665 (1969).
[3]J. Pascale and J. Vandeplanque, J. Chem. Phys. **60**, 2278 (1974).
[4]R. Duren, Adv. At. Mol. Phys. **16**, 55 (1980).
[5]R. P. Saxon and R. E. Olson, J. Chem. Phys. **67**, 2692 (1977).
[6]J. Pascale, Phys. Rev. A **28**, 632 (1983).
[7]D. D. Kanowalow, M. E. Rosenkrantz, and M. L. Olson, J. Chem. Phys. **72**, 2612 (1980).
[8]W. J. Stevens, D. D. Kanowalow, and L. B. Ratcliff, J. Chem. Phys. **80**, 215 (1984).
[9]G. Jeung, J. Phys. B **16**, 4289 (1983); Phys. Rev. A **35**, 26 (1987).
[10]A. Henriet and F. Masnou-Seeuws, J. Phys. B **20**, 671 (1987).
[11]The experimental literature regarding alkali-metal dimer molecules is vast [e.g., the bibliography in K. K. Verma, J. T. Bahns, A. R. Rajaei-Rizi, W. C. Stwalley, and W. T. Zemke, J. Chem. Phys. **78**, 3599 (1983)].
[12]M. Krause, Appl. Opt. **5**, 1375 (1966).
[13]A. Gallagher, Phys. Rev. **172**, 88 (1968).
[14]E. E. Nikitin and S. Ya. Umanski, in *Theory of Slow Atomic Collisions,* edited by W. McGowan (Springer-Verlag, New York, 1984), p. 317.
[15]W. D. Phillips and D. Pritchard, Phys. Rev. Lett. **33**, 1254 (1974).
[16]R. W. Anderson, T. P. Goddard, C. Parravano, and J. Warner, J. Chem. Phys. **64**, 4037 (1976).
[17]P. L. Gould, P. D. Lett, P. S. Julienne, W. D. Phillips, H. R. Thorsheim, and J. Weiner, Phys. Rev. Lett. **60**, 788 (1988), and references therein.
[18]R. H. G. Reid and A. Dalgarno, Phys. Rev. Lett. **22**, 1029 (1969); Chem. Phys. Lett. **6**, 85 (1970).
[19]W. B. Schneider, Z. Phys. **248**, 387 (1971).
[20]W. Gough, Proc. Phys. Soc. **90**, 287 (1967).
[21]M. X. Wang, M. S. de Vries, and J. Weiner, Phys. Rev. A **34**, 4497 (1986), and references therein.
[22]M. O. Hale, I. V. Hertel, and S. R. Leone, Phys. Rev. Lett. **53**, 2296 (1984).
[23]M. Movre and G. Pichler, J. Phys. B **10**, 2631 (1977).
[24]C. Vadla, C. J. Lorenzen, and K. Niemax, Phys. Rev. Lett. **51**,

988 (1983).
[25]W. D. Phillips, J. A. Serri, D. J. Ely, D. E. Pritchard, K. R. Way, and J. L. Kinsey, Phys. Rev. Lett. **41**, 937 (1978).
[26]R. Duren, E. Hasselbrink, and G. Hillrichs, Chem. Phys. Lett. **112**, 441 (1984).
[27]J. M. Mestdagh, P. de Pujo, J. Pascale, J. Cuvellier, and J. Berlande, Phys. Rev. A **35**, 1043 (1987).
[28]P. F. Liao, J. E. Bjorkholm, and P. R. Berman, Phys. Rev. A **21**, 1927 (1980).
[29]J. A. Serri, J. L. Kinsey, and D. E. Pritchard, J. Chem. Phys. **75**, 663 (1981).
[30]H. M. Srivastava and R. G. Buschman, *Convolution Integral Equations with Special Function Kernals* (Wiley, New York, 1977).
[31]K. Bergmann, U. Hefter, and P. Hering, Chem. Phys. **32**, 329 (1978).
[32]R. J. Gordon, Y. T. Lee, and D. R. Herschbach, J. Chem. Phys. **54**, 2393 (1971).
[33]L. Krause, in *The Excited State in Chemical Physics,* edited by W. McGowan (Wiley, New York, 1975), p. 267.